Proc. of CEES 2025 Construction, Energy, Environment and Sustainability. Volume 1: Construction Materials and Technologies. **Part of the book series:** Lecture Notes in Civil Engineering (LNCE, volume 743) Berardi et al. Eds. Springer **eBook ISBN**978-981-95-1822-7

Evaluation of Cement Mortars incorporating Calcined Red Mud: Characterisation and Strength Development

Gurbir Kaur [0000-0002-3307-6429], José María Fernández [0000-0003-3684-8778],
Íñigo Navarro-Blasco [0000-0003-1863-0580], Sara Pavia [0000-0003-4506-8386]
José Ignacio Álvarez [0000-0001-9170-7404]

[1,2,3,5] MATCH Research Group, Department of Chemistry, School of Sciences, University of Navarra, C/. Irunlarrea 1, 31008 Pamplona, Spain

[4] Dept of Civil Engineering. Trinity College Dublin, The University of Dublin, Ireland

gkaur@external.unav.es

Abstract

Transforming red mud, a waste product from aluminum production, into a valuable resource for construction industry offers manifold benefits: managing hazardous waste stockpiles, promoting sustainability in the building sector by decreasing cement consumption, environmental remediation. Red mud, a byproduct from the ALCOA San Ciprián industrial complex in Lugo, Spain, was subjected to calcination at two different temperatures. This process was conducted to enhance its reactivity, with the goal of utilizing it as a partial cement replacement in mortars. This study investigates the strength development of these mortars, considering two key variables: the substitution rate of red mud (fixed at 15% by weight of cement) and the calcination temperature of red mud (tested at both 300°C and 600°C). The investigated mortars are characterized using thermogravimetric and differential thermal analysis and X-ray diffraction techniques to provide valuable insights into their composition and properties. The results indicate that calcination induces changes in the crystalline structure of red mud; the phase transformation in calcined red mud involves conversion of mineral compounds like goethite to hematite, which results in more reactive red mud. The evolution of mortar strength is analysed in relation to the presence and proportions of crystalline phases within the mortars. These phases are examined as a function of three key factors: the temperature at which calcination occurs, and the duration of the curing process. This study also conducts an initial exploration into evaluating the photocatalytic potential of red mud for its possible use as a photocatalyst in cement-based materials. Transforming red mud, a waste product from aluminum production, into a valuable resource for construction industry offers manifold benefits: managing hazardous waste stockpiles, promoting sustainability in the building sector by decreasing cement consumption, environmental remediation.

Keywords: Calcined Red Mud, Photocatalytic Activity, Strength Development, Characterisation

1 Introduction - Overview and Research Objectives

Red mud, a byproduct of aluminum production, forms during the Bayer process when bauxite ore is refined into alumina. For every ton of alumina produced, 1–1.5 tons of this alkaline waste are generated [1], with global alumina production exceeded 135 million tons, resulting in approximately 200 million tons of red mud [2]. Current estimates suggest a global stockpile nearing 5 billion tons, highlighting the scale of this industrial challenge. Its high alkalinity (pH10–13) and potential contamination with heavy metals or radionuclides pose significant environmental risks if mismanaged. Improper storage can lead to groundwater contamination, soil degradation, and catastrophic spills, as seen in past incidents [3,4]. Despite challenges, red mud shows promise as a resource in sustainable construction. It is rich in iron, silica, alumina, and calcium oxides, which makes it suitable for cementitious applications, either as a partial cement replacement or in geopolymer binders. Red mud can meet both the strength and durability requirements of concrete, making it a viable replacement for traditional cement in various construction materials such as bricks, road substrates, and geopolymers [5]. It derives the reddish hue from iron oxides like hematite (Fe_2O_3) and goethite (FeOOH), which dominate its composition. Due to its high iron oxide content, red mud is suitable for producing colored architectural cementitious composites. The red coloration can be enhanced by calcination, making it a valuable pigment and functional additive. Red mud has also been proposed for creating eco-environmental materials capable of photocatalytically degrading indoor air pollutants, addressing both environmental pollution and indoor air quality [6]. It has shown effectiveness as a photocatalyst for the solar degradation of aquatic pollutants and the removal of contaminants like Cr (VI) and malachite green from wastewater [7]. Incorporating red mud into cementitious materials aligns with global sustainability goals by reducing reliance on traditional raw materials such as limestone and clay. Red mud-based cementitious composites can be designed to mimic historical building materials like red brick or sandstone, offering aesthetic benefits for restoring modern structures. By diverting red mud from landfills, this approach addresses waste management costs, minimizes mining impacts, and contributes to low-carbon building solutions.

This study focuses on utilization of red mud in the preparation of mortars. A key aspect of this research is the pre-treatment of red mud to enhance its reactivity. The study used red mud from a single source but subjected to incineration at two different temperatures (300°C and 600°C). This thermal treatment process is designed to alter the chemical and physical properties of red mud, potentially increasing its pozzolanic activity or its ability to react with cement hydration products. By comparing the performance of mortars incorporating these thermally treated red mud samples against a control group, authors aim to identify the optimal processing conditions that could make red mud a viable partial replacement for cement in mortar production, contributing to more sustainable construction practices. The experiment involved curing the mortar samples for two distinct periods - 7 days and 28 days - to evaluate the development of strength over time. This approach allows for a comprehensive understanding of how red mud affects the early and later stages of mortar strength development, which is crucial for determining its potential as a sustainable construction material. The mortars were analyzed using thermal and X-ray techniques to understand their composition. Additionally, the study preliminarily explores red mud's potential as a photocatalyst in cement-based materials.

2 Materials and methods

2.1 Materials and casting of mortar samples

In the present investigation, CEM III/A 42,5 N/SRC cement, marketed as 'Rezola FORTE', and EN 196-1 compliant siliceous standard sand were utilized to prepare mortars. Red mud, sourced from Alcoa San Ciprian in Lugo, Spain, was incorporated as a partial cement replacement, 15% by weight. Prior to its use as a partial cement substitute in mortar preparation, the red mud underwent incineration at two separate temperatures, 300°C and 600°C, with each thermal process lasting 3 hours. Based on the temperature conditions, incinerated red mud was subsequently designated as IRM300 and IRM600. Additionally, red mud oven dried at 105°C (RM105) was also used at same replacement to prepare mortar samples for both testing ages. The chemical composition of cement and three types of red mud was determined using X-ray Fluorescence (XRF) analysis, with results displayed in Table 1. A control mix was prepared using the standard 1:3 cement-to-sand proportion with a water-to-binder ratio of 0.5. Furthermore, three mixtures incorporating red mud were designed by replacing a fixed amount of cement in the control mix with different types of red mud. Prism samples measuring 40x40x160 mm were prepared to evaluate the compressive strength of the tested mortars at 7 days and 28 days. The specimens were cured at 20°C temperature and relative humidity greater than 95% until the designated testing ages.

2.2 Methods

2.2.1 Characterisation techniques

The mineralogical composition of red mud and mortars investigated in this study was determined by X-ray diffraction (XRD) using Bruker D8 Advance diffractometer. The data analysis was carried out using DIFFRACplusEVA® software from Bruker. The thermal analysis of red mud and mortar samples was performed using TA Instruments' TRIOS software. Samples of approximately 10 mg were loaded into alumina crucibles. The thermal program consisted of heating the samples from 35°C to 1100°C at a rate of 20°C/min.

2.2.2 Mechanical testing

To assess the mechanical properties of the investigated mortars, compressive strength tests were conducted after 7 and 28 days of curing. These tests were performed in accordance with the standards outlined in BS EN 1015-11:2019.

2.2.3 Photocatalytic activity

The ISO 22197-1:2007 test standard, which evaluates the photocatalytic materials for air purification based on their effectiveness in removing nitric oxide (NO), has been used to determine the photocatalytic potential of red mud. The test setup consists of a test gas supply, a photoreactor, a light source and pollutant (NO) measuring equipment. The photoreactor was fed by 500 ppb NO stream. The concentrations of NO and NO_X were determined by a chemiluminescence detector (Environnement AC32M) at a 0.78 $L \cdot min^{-1}$ flow. Following a 30-minute equilibration, samples were exposed to a 300 W Ultra Vitalux lamp for one hour for solar illumination. The application of an ultraviolet filter, which removed this portion of the spectrum, enabled the study of the samples under solar irradiation (UV + visible light) as well as under strictly visible light irradiation.

Table 1. Chemical composition of cement and red mud types used in the investigation.

Elements	CEMIII	RM105	IRM300	IRM600
CaO	58.39	3.44	3.32	3.43
MgO	3.81	0.34	0.28	0.44
Al_2O_3	7.47	16.33	16.21	16.10
SiO_2	21.22	7.01	7.00	6.81
Fe_2O_3	2.58	58.94	59.42	59.88
SO_3	4.25	0.49	0.51	0.50
K_2O	1.00	0.11	0.09	0.07
Na_2O	-	3.71	3.38	3.94
MnO	0.13	0.12	0.12	0.12
ZrO_2	0.03	0.34	0.36	0.29
TiO_2	0.50	8.30	8.42	7.61
V_2O_5	0.03	0.33	0.32	0.31
Cr_2O_3	0.03	0.32	0.32	0.32
Sc_2O_3	0.29	-	-	-

3 Results and Discussion

3.1 Characterization of red mud powders: XRD and TGA

The X-ray diffraction pattern for three types of red mud used in the investigation is shown in Fig. 1. Red mud typically reveals a complex mixture of mineral phases, and the prominent mineral phase observed in XRD patterns of red mud samples is hematite. The XRD analysis of incinerated red mud samples reveals that the mineral composition at 300°C and 600°C largely mirrors that of untreated red mud. However, as the temperature increases, subtle alterations in the mineral phases become apparent. For instance, heating red mud beyond 300°C initiates gibbsite ($Al(OH)_3$) conversion into boehmite (AlOOH) and amorphous aluminum oxide (Al_2O_3). This phase transition explains the absence of gibbsite peaks in the XRD pattern of IRM600 sample. Boehmite remains thermally stable under these conditions, as its dehydroxylation (loss of hydroxyl groups) primarily occurs above 450°C, with peak decomposition rates observed near 500°C [8,9]. Since the heat treatment at 300°C falls well below this threshold, boehmite retains its crystalline structure and remains detectable in the XRD analysis of IRM300. Other mineral phases remain largely unchanged at this temperature, as significant transformations occur at higher temperatures only. Also, the thermal decomposition of goethite (α-FeOOH) in red mud samples into hematite (α-

Fe_2O_3) typically begins around 280–320°C and completes by 420–500°C, depending on the presence of aluminum substitutions and other mineral phases [10]. For this reason, IRM600 does not contain goethite, as it may have been fully decomposed at 600°C. When red mud is heated to 600°C, goethite undergoes thermal decomposition, converting into hematite. The transformation process related to exact behavior of sodalite is a complex process and involves multiple reactions among the various components present in the red mud. However, around 600°C, sodalite begins to break down, altering the mineral composition of the red mud. As sodalite and other components decompose, the relative concentration of Fe_2O_3 in the remaining mass increases. The decomposition of calcite ($CaCO_3$) typically begins at higher temperatures i.e., it generally starts around 550-850°C. Consequently, the XRD patterns of all red mud samples shows calcite as main phase. The examination using XRD technique indicates that hematite is a dominant crystalline component present in all red mud samples. The calcination process enhances red mud particle dispersion and decomposes inert phases, potentially improving hematite visibility and its relative proportion in the investigated samples.

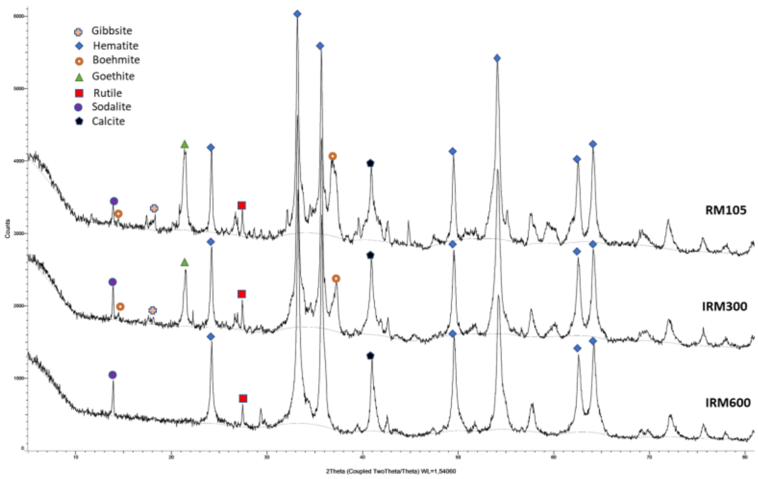

Fig. 1. XRD pattern of investigated red mud types.

Thermogravimetric analysis - differential thermal analysis (TG-DTA) technique was also used for identifying phase transformations in red mud samples, including the dehydroxylation of minerals such as gibbsite and goethite (Fig. 2). Table 2 illustrates the weight loss at important phase transformations in red mud samples as temperature rises. One of the main thermal events observed in Fig. 2 is decomposition of gibbsite, which is characterized by an endothermic peak for RM105 and IRM300 typically occurring between 334-338°C. As mentioned previously, this reaction entails the transformation of gibbsite into alumina, accompanied by the release of water molecules. While boehmite is often an intermediate product of gibbsite decomposition, it also begins to decompose further at temperatures approaching 400°C (specifically, 365-370°C observed more clearly in RM105 and IRM300). Peak around 250°C for red mud samples, corresponding to the thermal decomposition of goethite into hematite. The thermal transformation of goethite to hematite occurs due to dehydroxylation at about 200°C, with the proportion of hematite increasing with temperature. The weight loss associated with decomposition of goethite and gibbsite phases occurring between 200-400°C is more for RM105 (6.8%) and IRM300 (6.3%) as compared to IRM600 (1.8%).

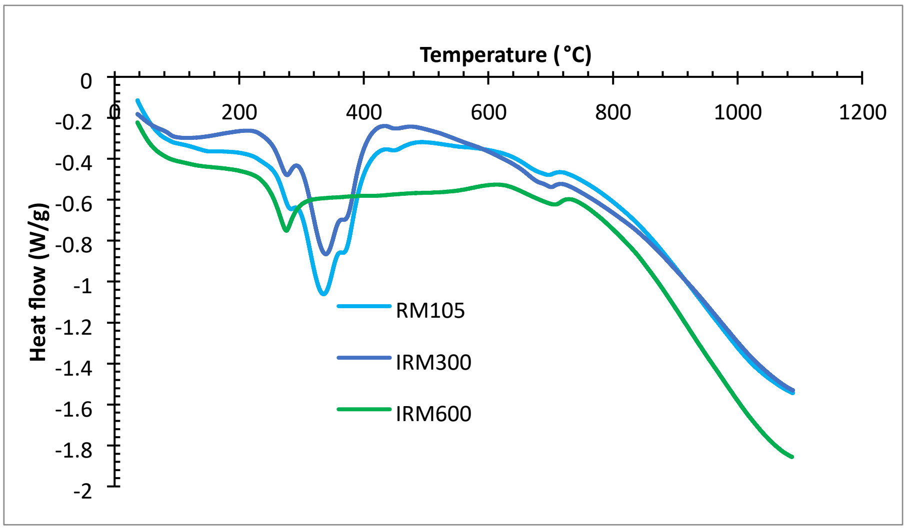

Fig. 2. TGA output of investigated red mud samples.

3.2 Compressive strength of mortars

Table 2 presents the compressive strength results of mortars at 7 days and 28 days of testing. Mortar mix containing 15% of oven dried red mud (i.e., R15-105) resulted in 23% drop in compressive strength of mix after 7 days of curing in comparison to control mix (21.56 MPa). The 7-day compressive strength performance of mortars containing red mud incinerated at 300°C (i.e., R15-300) reported 16% drop in the compressive strength with respect to control mix. For the case of mortars containing red mud incinerated at 600°C (i.e., R15-600), the compressive strength of R15-600 (19.90 MPa) remains lower than that of control mix. One typical observation is that the 7-day compressive strength of RM600 based mortars is relatively better than that of RM300 and RM105 counterparts, which is evident from the compressive strength of mortars containing higher dose of RM (i.e., 19.90>18.07>16.54 MPa). The results indicate that the thermal processing method applied to red mud, be it high-temperature incineration or low-temperature oven-drying, does not substantially affect the initial strength development of mortars when red mud is used as a 15% substitute. The trend in the 28-day compressive strength of mortar containing oven dried red mud remains same as that of 7-day compressive strength i.e., compressive strength drops with an increase substitution rate of red mud. Mortar R15-105 reported 44% drop in 28-day compressive strength as compared to control mix (37 MPa). It can also be concluded that incinerating red mud to 300°C and 600°C has not contributed to strength improvement of mortars. IRM300 based mortar reported 30% drop in the 28-day compressive strength and mortar containing IRM600 reduced the compressive strength by 31%. Red mud's performance is influenced by multiple factors, with chemical composition being the primary determinant of its alkalinity and pozzolanic properties. Its limited pozzolanic activity stems from low concentrations of silica (SiO_2) and calcium oxide (CaO), which are critical for reactivity. Additionally, impurities such as heavy metals and alkaline compounds may further reduce effectiveness by restricting silica availability during reactions. The high alkalinity of red mud, partly due to sodium oxide, has negative impact on the long-term strength development of mortars. Red mud, while potentially aiding particle packing as an inert filler, ultimately hinders the strength development due to its low pozzolanic reactivity, high alkalinity, and altered hydration dynamics. Furthermore, the addition of red mud effectively reduces the proportion of cement in the mixture, leading to a dilution effect. The combination of these factors ultimately results in a composite material with diminished strength performance compared to traditional cement formulations without red mud. Figs. 3 and 4 presents the hydration phases presents in mortars at 7 days and 28 days testing. The XRD analysis revealed that mortars incorporating red mud exhibited negligible crystalline hydration products associated with strength development, such as calcium silicate hydrate (C-S-H) phases. This suggests limited pozzolanic reactivity between the red mud components and calcium hydroxide, a critical process for generating binding phases in blended cement matrices. The absence of these key reaction products aligns with observed reductions in compressive strength, highlighting red mud's inert behavior as a partial cement substitute under standard curing conditions. Table 3 illustrates the phase transformations observed in the investigated mortars across three distinct stages. Stage 1 corresponds to the removal of water from hydrated products, including C-S-H and other cement phases. Stage 2 involves the dehydroxylation of various phases, while Stage 3 represents the decarbonation reaction. A larger mass loss in the temperature range 600–800°C (Table 3) suggests a higher content of calcite ($CaCO_3$) in the samples, this implies that more carbonation has occurred in the red mud-cement composites. The consumption of calcium hydroxide through carbonation can have both positive and negative effects on strength. Initially, it may contribute to early strength development, but excessive carbonation can lead to reduced long-term strength due to the depletion of calcium hydroxide needed for ongoing hydration reactions.

Table 2. Compressive strength of mortars in MPa

Sample ID	7-day compressive strength	28-day compressive strength
Control	21.56	37
R15-105	16.54	20.59

R15-300	18.07	25.78
R15-600	19.90	25.41

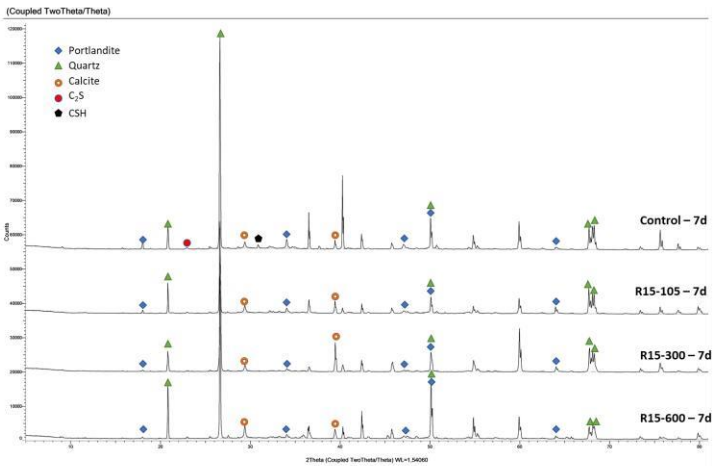

Fig. 3. XRD output of mortars at 7 days of curing.

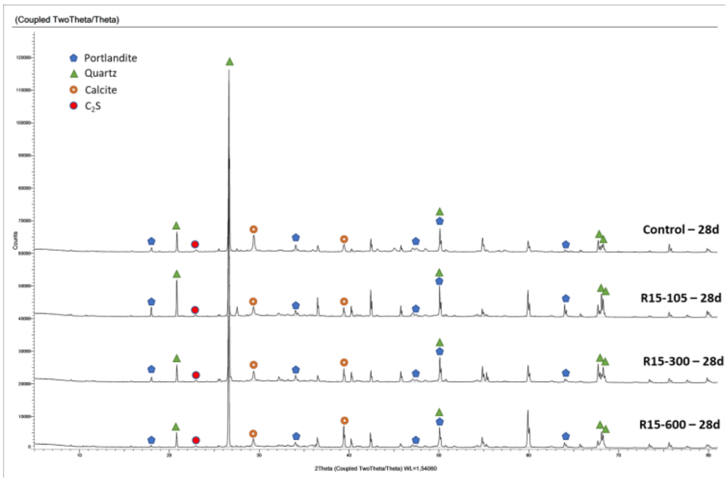

Fig. 4. XRD output of mortars at 28 days of curing.

Table 3. Normalised weight change for investigated mortars at 7 days and 28 days of curing – TGA output.

Mix	Stage 1 35°C -300°C	Stage 2 400°C-600°C	Stage 3 600°C-800°C
Control – 7d	3.501%	1.328%	1.428%
C3R15 – 7d	3.020%	0.990%	1.335%
C3R15-3 – 7d	2.447%	0.951%	1.692%
C3R15-6 – 7d	3.056%	0.142%	1.853%
Control – 28d	4.877%	1.030%	1.252%

C3R15 – 28d	3.282%	1.107%	1.677%
C3R15-3 – 28d	3.551%	0.872%	1.412%
C3R15-6 – 28d	3.694%	0.989%	1.840%

3.3 Photocatalytic Activity Test – Abatement of Nitrogen Oxides

Fig. 5 depicts the decrease in NO and NOx concentrations for each type of red mud under solar irradiation (UV + visible light) and under visible light-only irradiation. Samples labeled with the letter 'F' correspond to those tested exclusively under visible light conditions. The red mud powders exhibited photocatalytic activity, as evidenced by their partial degradation of NO. This catalytic behavior is attributed to the hematite (α-Fe_2O_3) identified in the chemical composition of red mud, which acts as a semiconductor to facilitate electron-hole pair generation under illumination. The demonstrated degradation of pollutants underscores the potential of red mud for use in environmental remediation and pollution management. The photocatalytic NO oxidation typically occurs in stages as depicted below:

$$NO \text{ (nitrogen oxide)} \rightarrow NO_2 \text{ (nitrogen dioxide)} \rightarrow NO_3^- \text{ (nitrate)}$$

The substantially suppressed NO_2 generation observed during NO abatement testing demonstrates progression of the reaction beyond intermediate nitrogen species, achieving effective oxidation of NO_2 to nitrate species (NO_3^-). This result confirms the photocatalytic efficacy of red mud in driving the secondary oxidation process under tested conditions. The observed transformation of NO to stable nitrate products demonstrates complete photocatalytic oxidation capability, indicating red mud's potential as a functional catalyst for advanced NOx remediation.

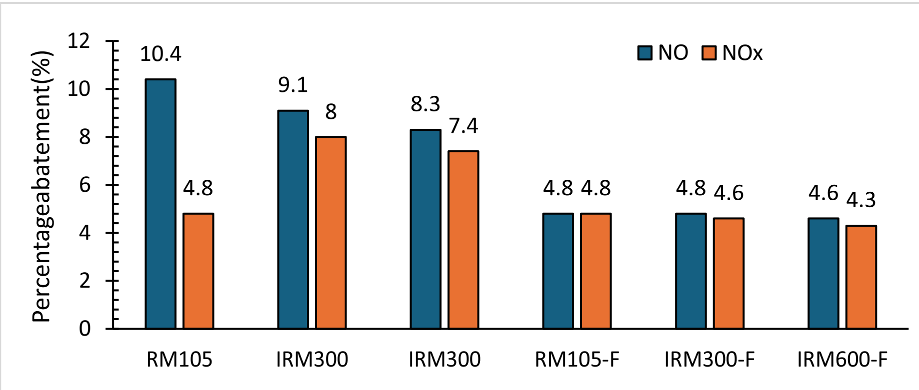

Fig. 5. NO and NOx abatement of oven-dried red mud and red mud calcined at 300°C and 600°C.

4. Conclusion

Red mud possesses a distinctive chemical composition, with its high hematite content making it a promising material for environmental remediation. However, its limited pozzolanic activity restricts its ability to enhance the strength development of mortars when used as a 15% cement replacement. Despite this limitation, red mud remains a viable option for applications such as repair work or scenarios requiring low to moderate strength mortars.

Acknowledgments. This research was funded by the European Union's Horizon 2020 research and innovation programme under the Marie Skłodowska-Curie grant agreement No 101034345 and the Ministerio de Ciencia e Innovación, grant number TED2021-129705B-C33 Terra-Cycle.

Disclosure of Interests. The authors have no conflicts of interest to disclose.

References

1. Jie Li, Lin Xu, Panpan Sun, Peiyan Zhai, Xiuping Chen, Heng Zhang, Zhaoshun Zhang, Wancheng Zhu: Novel application of red mud: Facile hydrothermal-thermal conversion synthesis of hierarchical porous AlOOH and Al2O3 microspheres as adsorbents for dye removal, Chemical Engineering Journal 321, 622-634 (2017).
2. Qianwen Tan, Qilin Yang, Chengsen Ye, Dawei Wang, Ning Xie: Utilization of red mud in high-performance grouting material for semi-flexible pavement, Journal of Cleaner Production 454, 142240 (2024).
3. Emile Mukiza, LingLing Zhang, Xiaoming Liu, Na Zhang: Utilization of red mud in road base and subgrade materials: A review, Resources, Conservation and Recycling 141, 187-199 (2019).
4. Jizhe Zhang, Zhanyong Yao, Kai Wang, Fei Wang, Hongguang Jiang, Ming Liang, Jincheng Wei, Gordon Airey: Sustainable utilization of bauxite residue (Red Mud) as a road material in pavements: A critical review, Construction and Building Materials 270, 121419 (2021).
5. Pei Yan, Bing Chen, M. Aminul Haque, Tianyu Liu: Influence of red mud on the engineering and microstructural properties of sustainable ultra-high-performance concrete, Construction and Building Materials 396, 132404 (2023).
6. Yidi Wang, Na Zhang, Chengqian Zhang, Ying Wang, Ping Lu, Yihe Zhang: Utilising bauxite residue (red mud) to construct Z-type heterojunction for formaldehyde degradation, Journal of Cleaner Production 444, 141280 (2024).
7. Dilip D. Sarode, Chapter 9 - Use of industrial waste for value-added products, Editor(s): Sarika Verma, Raju Khan, Medha Mili, S.A.R. Hashmi, Avanish Kumar Srivastava, Advanced Materials from Recycled Waste, pp. 179-198. Elsevier, (2023).
8. Morsy M. Abou-Sekkina, Salah A. Abo-El-Enein, Nagy M. Khalil, Osama A. Shalma: Phase composition of bauxite-based refractory castables, Ceramics International 37(1), 411-418, (2021).
9. Yuanfeng Cai, Xiang Li, Xiumian Hu, Xiaoming Chen, Yuguan Pan: Paleoclimatic approach to the origin of the coloring of Turonian pelagic limestones from the Vispi Quarry section (Cretaceous, central Italy), Cretaceous Research 30(5), 1205-1216 (2009).
10. Shrey Agrawal, Nikhil Dhawan: Investigation of carbothermic microwave reduction followed by acid leaching for recovery of iron and aluminum values from Indian red mud, Minerals Engineering 159, 106653 (2020).